JAMES | Journal of Advances in Modeling Earth Systems

RESEARCH ARTICLE
10.1029/2019MS001772

Response of Convective Boundary Layer and Shallow Cumulus to Soil Moisture Heterogeneity: A Large-Eddy Simulation Study

Cunbo Han[1,2,3], **Slavko Brdar**[1,3,4], **and Stefan Kollet**[1,3]

[1]Institute for Bio- and Geosciences: Agrosphere (IBG-3), Research Centre Jülich, Jülich, Germany, [2]Now at Institute of Meteorology and Climate Research (IMK-TRO), Karlsruhe Institute of Technology, Karlsruhe, Germany, [3]Centre for High-Performance Scientific Computing in Terrestrial Systems, Geoverbund ABC/J, Jülich, Germany, [4]SimLab TerrSys, Jülich Supercomputing Centre, Research Centre Jülich, Jülich, Germany

Key Points:

- The higher soil moisture variance the more available energy is partitioned into latent heat flux, while the domain-averaged soil moisture is identical
- Liquid water path increases, while cloud cover decreases with stronger soil moisture structure and increasing soil moisture variance
- The impact of shallow cumulus clouds on domain-averaged surface net radiation is not significant

Correspondence to:
C. Han,
cunbo.han@hotmail.com

Citation:
Han, C., Brdar, S., & Kollet, S. (2019). Response of convective boundary layer and shallow cumulus to soil moisture heterogeneity: a large-eddy simulation study. *Journal of Advances in Modeling Earth Systems*, *11*, 4305–4322. https://doi.org/10.1029/2019MS001772

Received 3 JUN 2019
Accepted 29 OCT 2019
Accepted article online 7 NOV 2019
Published online 13 DEC 2019
Corrected 13 APR 2020

This article was corrected on 13 APR 2020. See the end of the full text for details.

Abstract In this study, the impact of varying soil moisture heterogeneity (spatial variance and structure) on the development of the convective boundary layer and shallow cumulus clouds was investigated. Applying soil moisture heterogeneity generated via spatially correlated Gaussian random fields based on a power law model and idealized atmospheric vertical profiles as initial conditions, three sets of large-eddy simulations provide insight in the influence of soil moisture heterogeneity on the ensuing growth of the convective boundary layer and development of shallow cumulus clouds. A sensitivity on the strong, weak, and unstructured soil moisture heterogeneity is investigated. The simulation results show that domain-averaged land surface sensible heat and latent heat flux change strongly with changing soil moisture variance because of the interactions between surface heterogeneity and induced circulations, while domain means of soil moisture are identical. Vertical profiles of boundary layer characteristics are strongly influenced by the surface energy partitioning and induced circulations, especially the profiles of liquid water and liquid water flux. The amount of liquid water and liquid water flux increases with increasing structure. In addition, the liquid water path is higher in case of strongly-structured heterogeneity because more available energy is partitioned into latent heat and more intensive updrafts exist. Interestingly, the increase of liquid water path with increasing soil moisture variance only occurs in the strongly structured cases, which suggests that soil moisture variance and structure work conjunctively in the surface energy partitioning and the cloud formation.

Plain Language Summary The land surface is heterogeneous with respect to, for example, land use, plant cover, soil moisture, and topography over a wide range of spatial scales, which strongly influences the atmospheric boundary layer. In this study, the impact of soil moisture heterogeneity on the development of the convective boundary layer and shallow cumulus clouds was investigated. The results from a series of large-eddy simulations show that soil moisture heterogeneity impacts significantly on the surface energy partitioning, the convection boundary layer development and the cloud formation. Interestingly, the stronger soil moisture heterogeneity, the more available energy is partitioned into latent heat flux and the higher liquid water path in the atmosphere.

1. Introduction

Shallow cumulus convection plays an important role in determining the vertical thermodynamic structure of the atmosphere and influences the large-scale circulation in both the tropics and midlatitudes. This type of convection intensifies the vertical turbulent transport of momentum, heat, and moisture and, as a result, deepens the cloudy boundary layer and enhances significantly surface evapotranspiration (Siebesma et al., 2003). Terrestrial nonprecipitating shallow cumulus clouds are tightly coupled with the underlying land surface. These cumulus clouds represent an early stage in the development of deep convection and also play an essential role in the coupled land-atmosphere system. Based on observations and numerical simulations, previous studies showed that heterogeneous heating of the atmosphere by the land surface may generate a mesoscale circulation which influences the development of convective boundary layer (CBL) and the formation of clouds (Avissar & Schmidt, 1998; Bosman et al., 2018; Golaz et al., 2001; H.-Y. Huang & Margulis, 2011; Lee et al., 2019; Patton et al., 2005; Pielke, 2001; Rieck et al., 2014; Rochetin et al., 2017). Therefore,

understanding the processes, which govern the interactions among a heterogeneous land surface, CBL structure, and shallow cumulus convection, is of crucial importance.

Large-eddy simulation (LES) has been used to study land-atmosphere interactions and the impact of the land surface heterogeneity on atmospheric boundary characteristic (Avissar & Schmidt, 1998; Hadfield et al., 1991, 1992; Han et al., 2019; Patton et al., 2005; Raasch & Harbusch, 2001; Shen & Leclerc, 1995; Sühring et al., 2014; van Heerwaarden et al., 2014), on the shallow convection development (H. Y. Huang & Margulis, 2013; Kang & Ryu, 2016; Raasch & Harbusch, 2001; van Heerwaarden & de Arellano, 2008) and on the transition from shallow to deep convection (Kang & Bryan, 2011; Lee et al., 2019; Rieck et al., 2014; Rochetin et al., 2017) for the past two decades. One main concern of these studies has been the optimal heterogeneity scale to induce a mesoscale circulation, which is commonly suggested to be at a mesoscale but varies considerably. Avissar and Schmidt (1998) reported that surface heterogeneity continually intensified the organized circulations as the heterogeneity scale increased from 2 to 40 km with prescribed surface fluxes. Shen and Leclerc (1995) and Raasch and Harbusch (2001) , also using prescribed surface fluxes, found that in case of small-scale, one-dimensional (1-D), and stripe-like heterogeneity, the intensity of the mesoscale circulations increased when the horizontal scale of the heterogeneity increased to about the boundary layer height. Using an LES and land surface model (LSM) coupled model, Patton et al. (2005) found that the optimal scale to induce a mesoscale circulation was 4 to 9 times the boundary layer height with 1-D, stripe-like heterogeneity in soil moisture. With an LES and LSM coupled model and continuous soil moisture variations, Han et al. (2019) reported that the optimal scale for horizontal transport was about 18 times the boundary layer height, while the optimal scale for vertical motions was about 2 times the boundary layer height. Recently, Lee et al. (2019) studied the effect of heterogeneity scale on the transition to deep convection by prescribing 2-D chessboard surface flux patches. They found that transition only occurred when patch size $\geq$5 km, and they attributed this to the formation of a moisture pool over dry patches due to the generated mesoscale circulation. Rieck et al. (2014) also investigated the response of transition to deep convection to the surface heterogeneity size by prescribing leaf area index in an LES and LSM coupled system. They found that in case of intermediate heterogeneity, size of 12.8 km produced the fastest transition from shallow to deep convection.

In addition to the heterogeneity length scale, the heterogeneity amplitude can modify the mesoscale circulation (Avissar & Schmidt, 1998; van Heerwaarden et al., 2014; van Heerwaarden & de Arellano, 2008), which in turn triggers an earlier onset of convection (Kang & Bryan, 2011) and even a transition from shallow to deep convection (Kang & Ryu, 2016). Several studies have reported that the mesoscale circulation intensity increases with increasing heterogeneity amplitude (Avissar & Schmidt, 1998; Patton et al., 2005; van Heerwaarden & de Arellano, 2008). van Heerwaarden et al. (2014) reported that the optimal state of mesoscale circulation is strongly related to the heterogeneity amplitude and stronger amplitudes result in an earlier optimal state by prescribing square patches of surface fluxes. Kang and Bryan (2011) investigated the effect of 1-D sinusoidal surface heat fluxes of various amplitudes on the moist convection. They found that as the amplitude becomes larger, the area of near-surface convergence becomes narrower and stronger and leads to an earlier transition to deep convection. Rochetin et al. (2017) showed that the presence of a strong surface sensible heat flux heterogeneity not only leads to an earlier triggering of deep convection but also affects the spatial distribution of the convection, where clouds mostly form over the hot surface by the induced mesoscale circulation.

Large-scale synoptic conditions such as the background wind could mask out the effects of land surface heterogeneities and exert an opposite impact on the development of the mesoscale circulation. Dörnbrack and Schumann (1993) reported that the influence of land surface heterogeneities is dramatically reduced in the presence of a weak background wind. Avissar and Schmidt (1998) showed that the induced mesoscale circulations are eliminated by a background wind speed of 5 m/s or higher. By adopting observed surface heat fluxes and varying background winds, Maronga and Raasch (2013) found that the mesoscale circulation pattern could not be directly linked to the underlying sensible heat flux pattern for background wind speeds of 3–6 m/s. Lee et al. (2019) reported that the background winds have a strong influence on the mesoscale circulation such that any wind stronger than 2 m/s effectively eliminates the impact of surface heterogeneity and brings no mesoscale circulation and leads no transition from shallow to deep convection.

Studies verified that surface characteristics strongly affect the land surface energy budget partitioning (Margulis & Entekhabi, 2001; Niyogi et al., 1999; Santanello et al., 2007), but the soil moisture appears to

be of particular importance (Desai et al., 2006; Zhang & Anthes, 1982). The interactions between soil moisture and CBL development have been the focus of many observational (Findell & Eltahir, 2003b; Santanello et al., 2018; Taylor et al., 2011) and modeling studies (Chen & Avissar, 1994; Ek & Holtslag, 2004; Findell & Eltahir, 2003a; H.-Y. Huang & Margulis, 2011). Findell and Eltahir (2003b) and Taylor et al. (2011) reported that deep convection initiation enhanced over heterogeneous soil moisture patterns in the Sahel area by analyzing satellite observations. Using LES initialized with prescribed surface sensible and latent surface fluxes, Golaz et al. (2001) found nearly no change in cloud cover over a very narrow soil moisture range of about 47% relative wetness. However, they found a large difference in boundary layer characteristics, cloud base and cloud top over wet and dry soils. H.-Y. Huang and Margulis (2011) investigated the impact of soil moisture and atmospheric stability on cloud development using a coupled LES and LSM and found that cloud cover fraction increases with increasing soil moisture only in case of strong atmospheric stability, while the opposite has been observed in case of weak atmospheric stability. Chlond et al. (2014) investigated the effect of soil moisture on the development of shallow cumulus convection and found that soil moisture and cloud cover coupling are positive in most of the cases. Using a cloud resolving model with prescribed dry and wet patches in soil moisture, Chen and Avissar (1994) found that land surface soil moisture affects the timing of onset of clouds and the intensity and distribution of precipitation. Cioni and Hohenegger (2017) investigated the effect of soil moisture on deep convections using an LES and LSM coupled system and found that convections are triggered earlier over dry soils than over wet soils under certain conditions, while total precipitation is always lower over dry soils.

While numerous LES studies have been performed, very few studies have documented the effect of the spatial variance and structure of soil moisture on the surface energy partitioning and the development of shallow cumulus convection using an LES and LSM coupled system. Three sets of analytic soil moisture fields are created with the spectral slopes increased from 0 to −3, that is, from unstructured and weak to strong structured heterogeneity. In addition, the domain means of soil moisture are persevered, while spatial variance is varying in each set. Two research questions are of particular interest: "How does the spatial variance and structure in soil moisture affect the partitioning of available energy into surface sensible and latent heat fluxes?" and "How does the surface energy partitioning affect the structure of the cumulus-topped boundary layer?". This includes the influence of surface heat fluxes on the structure of cumulus clouds, such as cloud base and cloud thickness, cloud fraction, liquid water path (LWP), and in-cloud turbulence. A series of idealized numerical experiments initialized with soil moisture patterns generated via spatially correlated Gaussian random fields using a power law model and prescribed atmospheric vertical profiles were performed to address these questions.

This paper is organized as follows: In section 2, we introduce our model setup and the experiment design; section 3 presents results and discussion; and section 4 includes a summary and conclusions.

2. Methodology

2.1. Model Description

Our primary tool is the large-eddy version of the icosahedral nonhydrostatic model (ICON-LEM) (Dipankar et al., 2015; Zängl et al., 2015). ICON-LEM is a fully compressible model and has been developed collaboratively between the German weather service (Deutscher Wetterdienst, DWD) and the Max Planck Institute for meteorology. ICON-LEM solves the prognostic variables on an unstructured triangular grid with C-type staggering based on a successive refinement of a spherical icosahedron (Dipankar et al., 2015; Wan et al., 2013; Zängl et al., 2015), in such a way that the singularity at the poles would be avoided. Governing equations are described in Wan et al. (2013) and Zängl et al. (2015).

A three-dimensional subgrid-scale turbulence parameterization based on the diagnostic Smagorinsky scheme is implemented in ICON-LEM. The scheme takes the modifications for thermal stratification by Lilly (1962) into account. A double-moment microphysics scheme based on Seifert and Beheng (2001) is also implemented in ICON-LEM. Instead of the default diagnostic cloud fraction scheme, a simple all-or-nothing scheme (Sommeria & Deardorff, 1977) is used that assumes that the cloud fraction within a grid box is either 1 or 0 and does not account for fractional cloud cover at the subgrid scale. The advection scheme for tracer in ICON-LEM uses the second-order upwind scheme by Miura (2007) in horizontal direction and third-order piecewise parabolic method by Colella and Woodward (1984) in vertical direction. The default artificial

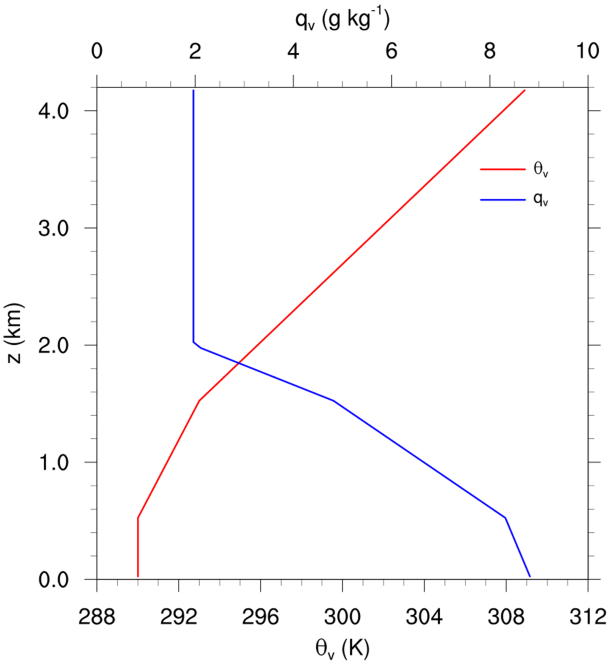

Figure 1. Initial profiles of potential temperature and specific humidity.

numerical dissipation for LES studies is reduced to fourth order in the momentum equations for numerical stability.

The multilayer land surface scheme Terra TERRA-Multi-Layer [TERRA-ML] without subgrid-scale variability is used in ICON-LEM (Schrodin & Heise, 2002). TERRA-ML provides momentum, heat, and moisture fluxes as boundary conditions for ICON-LEM and also predicts vertical profiles of soil moisture and temperature applying a one-dimensional set of equations for soil hydrologic and thermodynamic variables. The vertical soil water transport between layers is parameterized using Richards equation (Richards, 1931), and the soil temperature is calculated using a simplified heat diffusion equation. At the land surface, the biosphere-atmosphere transfer scheme formulation (Dickinson, 1984) is applied to estimate the bare soil evaporation and plant transpiration. As we focused on the development of CBL above the bare soil, only the theory of surface heat fluxes over a bare soil is described below. The surface sensible heat flux is defined accordingly:

$$H_{sfc} = -\rho C_h U\left(\theta\pi_{sfc} - T_{sfc}\right) \tag{1}$$

where ρ is air density, C_h is the bulk aerodynamical transfer coefficient for heat, U is the absolute horizontal wind velocity, θ and π_{sfc} are the air potential temperature at the lowest model level, and the scaled pressure at the ground surface, T_{sfc}, is the ground surface temperature. The bare soil evaporation, E_b, is calculated using the assumption $E_b = \mathrm{Min}\,(E_p; F_m)$, where E_p is potential evaporation and F_m is the maximum moisture flux through the surface that the soil can sustain. The parameterization formulae for E_p and F_m are given by:

$$E_p = -\rho C_q U\left(q - q_{sat}\left(T_{sfc}\right)\right) \tag{2}$$

$$F_m = C_k D \frac{s_0}{\left(z_0 z_1\right)^{1/2}} \tag{3}$$

where C_q is the bulk aerodynamical transfer coefficient for moisture, q is the specific humidity at the lowest grid level above the ground and q_{sat} is the saturated specific humidity at the ground surface, s_0 is the average soil water content in the total active layer divided by the soil pore volume, z_0 is the corresponding depth of the total active soil layer and z_1 is the depth of the surface soil layer, and C_k and D are parameters depending on the soil type and whose details could be found in Dickinson (1984).

2.2. Simulation Setup

In order to study the response of the CBL and cumulus clouds to soil moisture heterogeneity, a series of experiments were designed using an idealized configuration of the coupled ICON-LEM and TERRA-ML. The horizontal domain covers a mesoscale area of 19.2 × 19.2 km^2 with lateral double periodic boundary conditions and a horizontal grid spacing of 50 m. In the vertical direction, the first level is 20 m high, whereas all other levels have 50 m height up to a model top of 4.2 km. A 0.5 s time step was used. The initial profiles of potential temperature and specific humidity are shown in Figure 1; zero wind was imposed horizontally at the initial time step. The initial profiles were adapted from the work of Patton et al. (2005) with a conditionally unstable stratification. The only external forcing of the system was specified through the downward shortwave radiation, which was set to a constant value of 700 W/m^2 for all cases. Constant incoming shortwave radiative forcing at the model top limits the interaction between cloud and radiation and also leads to no diurnal cycle in radiation. However, it is a widely used configuration in idealized LES simulations and allows us to focus on the interactions between land surface and atmosphere. Random perturbations were added to the potential temperature field up to a height of 300 m to trigger the turbulence. A damping layer was applied close to the domain top to reduce the reflection and buildup of gravity waves.

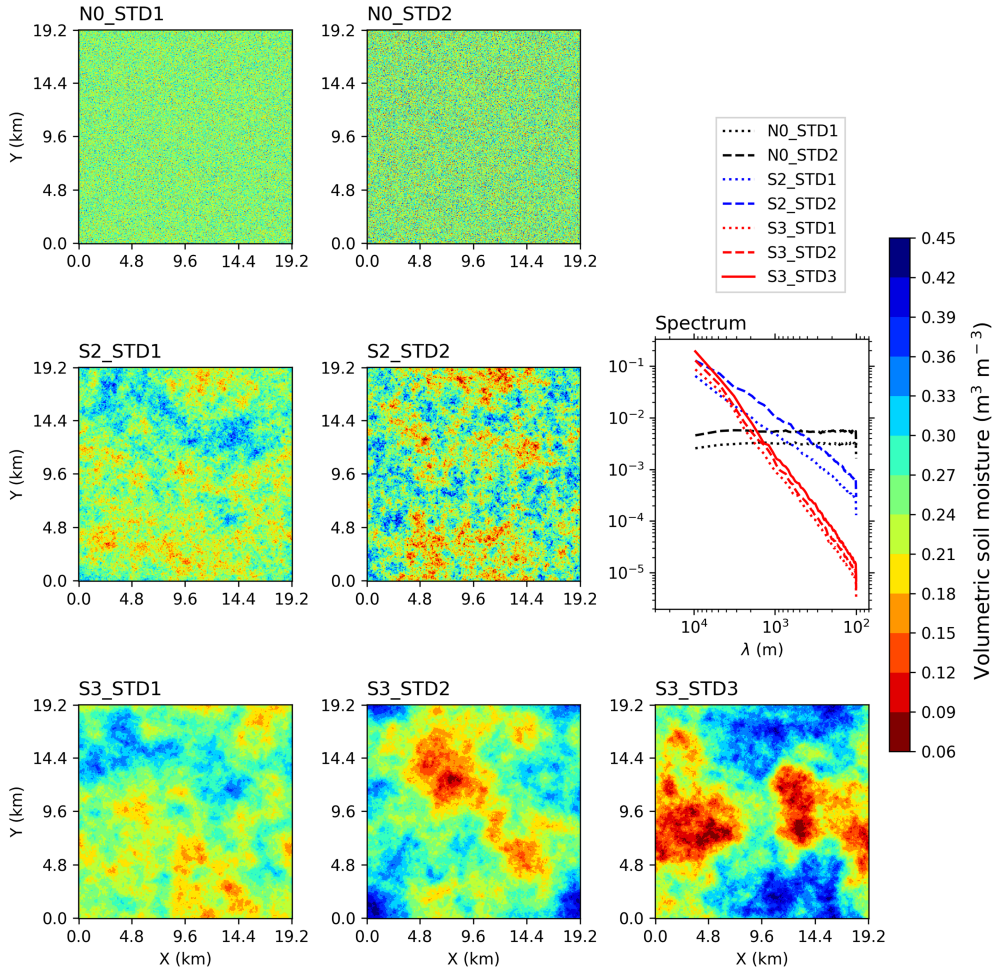

Figure 2. Spatial distributions of volumetric soil moisture and spectra for the seven cases at the initial time step, where λ is the wavelength.

In TERRA-ML, the soil column is discretized into eight soil layers. The soil type was uniform in space and was set to loam. The initial soil temperature profile was interpolated linearly from 290.4 K near the surface to the climatological value of 282.1 K at the lowest model layer. This setup corresponds to the most common soil type used in ICON-LEM model over a midlatitude area (e.g., Germany).

The soil moisture heterogeneity was generated applying spatially correlated Gaussian fields with a geostatistical toolkit developed by Heße et al. (2014). The spatial distributions and domain-averaged statistics of the soil moisture patterns are shown in Figure 2 and Table 1, respectively. The soil moisture maps have multiscale heterogeneities composed of harmonics in the same wavelength range. While the amplitude of each harmonic wavelength differs depending on the spectral slope, as shown in Figure 2, the soil moisture fields generated with a steeper −3 power spectral slope are dominated by large-scale heterogeneities compared to soil moisture fields with a −2 spectral slope. For reference, two quasi-homogeneous cases containing only white noise without any spatial structure were generated, that is to say, 0 spectral slope (Figure 2). Thus, we will refer to the soil moisture fields generated with −3, −2, and 0 slopes as strong, weak, and unstructured soil moisture heterogeneities, respectively. We regard the change characteristic of power spectral density with wavelength as the structure of the soil moisture heterogeneity. In addition, we created soil moisture fields of different variances (from STD1 to STD3) for each group of same spectral slope. In this study, we quantify the soil moisture heterogeneity with both structure and spatial variance. Note that the domain means (55% of the saturation value) are identical in all cases, and the same soil moisture values were applied to the entire soil column and were kept constant during the simulations. Detailed information for each case is listed in Table 1.

Table 1
Domain-Averaged Statistics for the Four Cases. Domain-Averaged Soil Moisture (AVG), Standard Deviation (STD), and Spectral Slope (Slope)

Setup	AVG (m^3/m^3)	STD (m^3/m^3)	Slope
N0_STD1	0.250	0.040	0
N0_STD2	0.250	0.060	0
S2_STD1	0.250	0.040	−2
S2_STD2	0.250	0.060	−2
S3_STD1	0.250	0.040	−3
S3_STD2	0.250	0.060	−3
S3_STD3	0.250	0.080	−3

3. Results and Discussion

Simulations of the seven cases were integrated for 6 hr, and the simulation results from $t = 2$ to 6 hr were used for analysis. Results were used to study the influence of soil moisture heterogeneity on CBL characteristics and cloud properties.

3.1. Surface Heat Fluxes

Figure 3 depicts the temporal evolution of domain-averaged net radiation flux, ground heat flux, surface sensible heat flux, latent heat flux, and Bowen ratio. An overview shows that the domain-averaged values of net radiation and ground heat flux are not influenced much by the interaction between heterogeneous soil moisture and the CBL. The differences in the sensible heat flux, latent heat flux, and Bowen ratio are stronger between cases of different variances, while in the case of same variance but different spectral slope, the difference is negligible. There is almost no difference in surface energy partitioning between the two unstructured cases (N0_STD1 and N0_STD2).

The spatial distribution of the land surface net radiation is strongly influenced by the clouds and negatively correlated with spatial distribution of LWP (Figure 4). The cloud covers and LWPs from the seven cases are significantly different from each other, while differences in domain-averaged net radiation are not obvious (Figure 3a). Domain-averaged cloud covers are high and LWPs are low in unstructured cases, while domain-averaged cloud covers are low and LWPs are high in structured cases (Figure 5). The influence of cloud cover is compensated by the influence of LWP when the net radiation fluxes are averaged over the domain. Hence, there are no obvious differences in domain-averaged net radiation. Besides, domain-averaged available heat fluxes, which are sensible heat flux plus latent heat flux, are almost identical. Thus, the domain-averaged ground heat flux does not vary between different cases.

Domain-averaged sensible heat fluxes decrease with increasing soil moisture variance (from STD1 to STD3), while surface latent heat fluxes increase with increasing soil moisture variance. Moreover, impacts on surface sensible heat flux, latent heat flux, and thus the Bowen ratio become more pronounced as simulation time increases (Figure 3). The results indicate that the higher soil moisture spatial variance, the more surface energy is partitioned into latent heat in the structured cases. In order to understand why the surface energy partitioning depends on the soil moisture variance, probability density functions (PDFs) of sensible heat flux, latent heat flux, net radiation flux, and soil moisture were generated (Figure 6). The PDF of soil moisture is wider, and a higher percentage of wet patch and dry patch exist in case of high soil moisture variance to maintain the high variance value (Figure 6d). Due to the nonlinear relationship between soil moisture and latent heat flux based on the surface layer similarity theory, extreme values of latent heat flux are generated over the wet and dry patch (Figure 6b) and contribute nonlinearly to the domain means. Figure 7 shows the bivariate PDFs between latent heat flux and soil moisture. Over the dry patches, with soil moisture smaller than 0.2 m^3/m^3, latent heat flux values are relatively low that do not contribute significantly to the domain means. Over the wet patches, especially where soil moisture larger than 0.3 m^3/m^3, latent heat flux values are quite high, which are about 300 W/m^2. Latent heat flux values increase almost linearly from about 10 to 300 W/m^2 as soil moisture increases from 0.2 to 0.3 m^3/m^3. Thus, a few points on the wet side of soil moisture increase strongly the domain-averaged latent heat flux. This is the reason why with higher soil moisture variance, more available energy is partitioned into latent heat flux, and explains why the surface energy partitioning is different, while domain means of soil moisture are identical.

To investigate the temporal evolution of the spatial distribution of surface heat fluxes and mesoscale circulation patterns, Figure 8 depicts spatial distribution of hourly averaged horizontal wind at the lowest model level and land surface sensible heat flux at hours 1, 2, 3, 4, 5, and 6 for case S3_STD3 which is the strongly structured case and has the largest soil moisture spatial variance. The spatial pattern of surface sensible heat flux is maintained over the six simulation hours due to constant soil moisture values in time. However, the magnitude of sensible heat flux changes with time due to the induced mesoscale circulation. During the first simulation hour, the mesoscale circulation is building up, and no horizontal wind velocity is larger than 2 m/s (Figure 8a). From the second simulation hour, the mesoscale circulations are well established

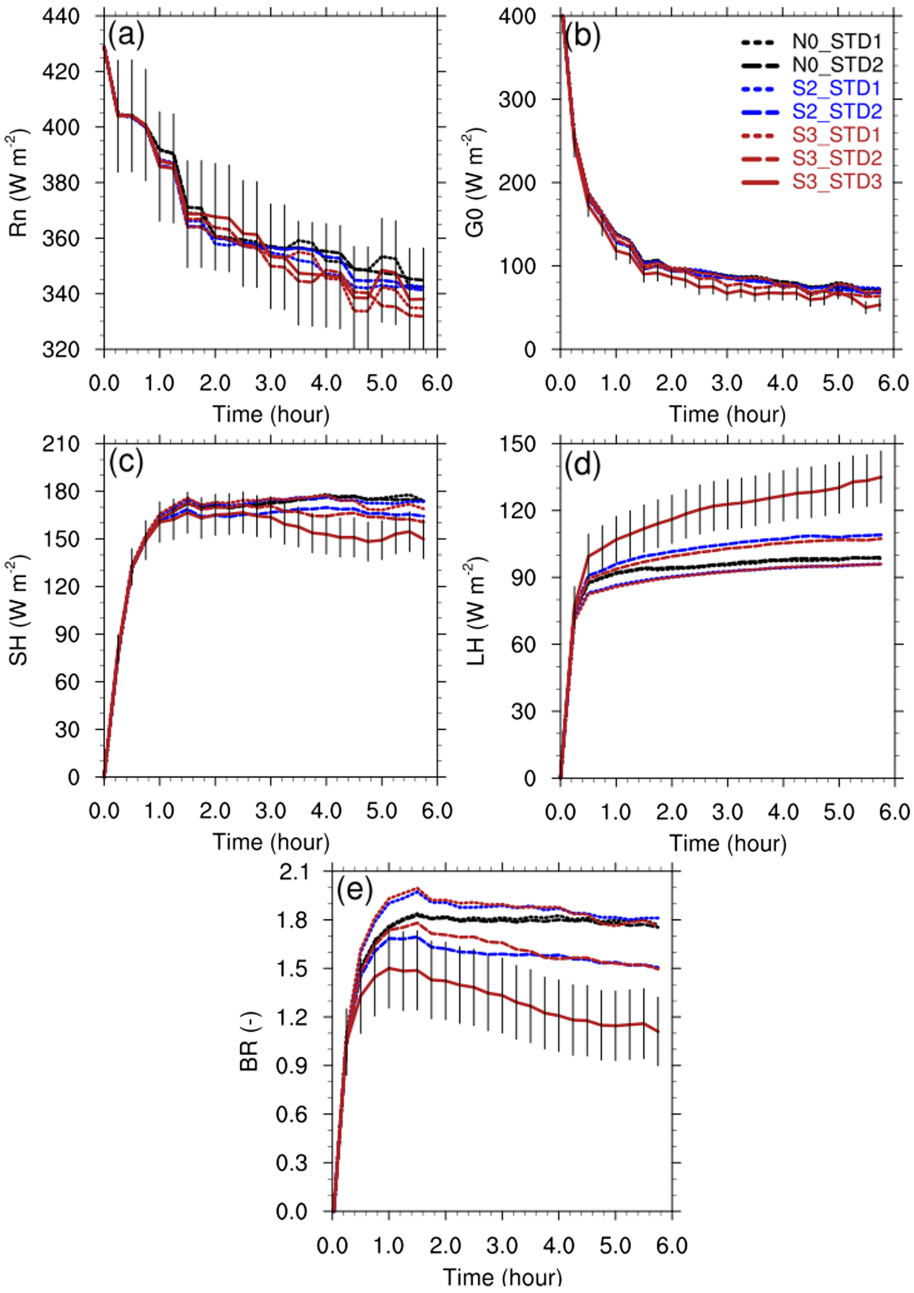

Figure 3. Time evolution of the domain-averaged surface (a) net radiation, (b) ground heat lux, (c) sensible heat flux, (d) latent heat flux, and (e) Bowen ratio. Error bars showing the standard deviation for case S3_STD3.

(Figure 8b). During 4 to 6 hr, strong convergence zones and updrafts have been established, where horizontal wind velocity is low and surface sensible heat flux is weak (Figures 8d–8f).

3.2. Vertical Profiles

In this section, we investigate the influence of two-dimensional surface heterogeneity on the dynamics and thermodynamics of the cumulus-topped CBL.

3.2.1. Vertical Profiles of Boundary Layer States and Fluxes

Figure 9 shows the domain- and time-averaged vertical profiles of potential temperature, specific humidity, liquid water mixing ratio, buoyancy flux, total water vapor flux, and liquid water flux. Profiles of potential

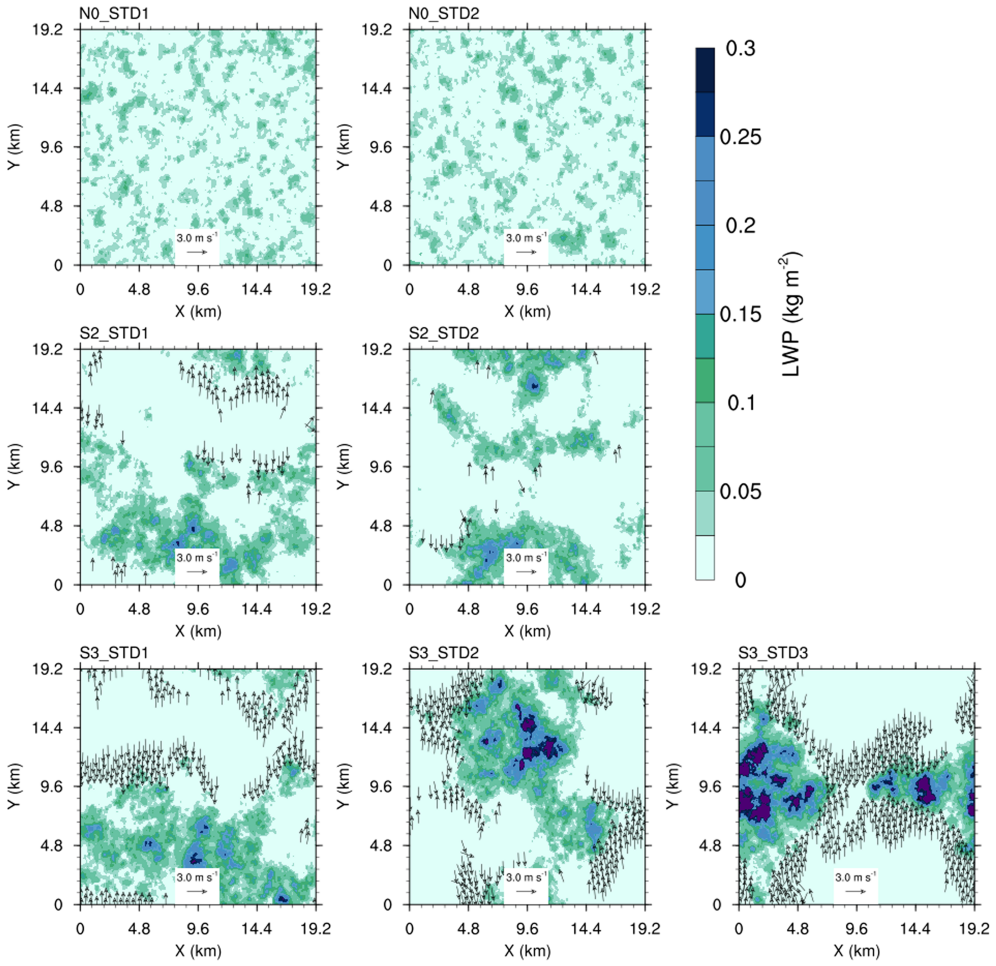

Figure 4. Spatial distribution of LWP and horizontal wind at the lowest model level (arrows). The quantities were averaged over the time period t = 2 to 6 hr. Only wind vectors with velocity larger than 2 m/s are plotted.

temperature and specific humidity show a typical CBL structure of a well-mixed boundary layer between the surface and the entrainment layer where strong gradients of potential temperature and specific humidity occur.

Comparison of potential temperature profiles depicted in Figure 9a shows that the profiles are almost identical for the heterogeneous soil moisture cases, while the potential temperature profile of the unstructured cases are better mixed and have a slightly stronger inversion layer compared to the structured cases. Vertical profiles of buoyancy flux are shown in Figure 9d. The surface with larger soil moisture variance provides a lower sensible heat flux. All the buoyancy fluxes decrease from a maximum value close to the surface and reach a minimum value at the entrainment layer, representing a characteristic behavior of the CBL. The buoyancy flux difference between unstructured cases and structured cases is small below the entrainment layer and becomes significant near the entrainment zone, and the difference is as much as 20 W/m^2. The difference in entrainment flux can be attributed to the influence of the induced mesoscale circulation and has been reported previously by several studies (Han et al., 2019; Sühring et al., 2014). Moreover, the buoyancy flux difference is pronounced in the cloud layer due to the different rates of entrainment in clouds between different cases.

Vertical profiles of specific humidity are illustrated in Figure 9b. In the lower portion of the mixed layer, specific humidity is highest in case S3_STD3 and specific humidity profiles are almost identical in other cases. In the upper portion of the mixed layer, the specific humidity decreases from unstructured to strongly structured cases. Vertical profiles of moisture flux are shown in Figure 9e. Moisture fluxes are almost identical between different cases, except the moisture flux of case S3_STD3, which is slightly higher close to the

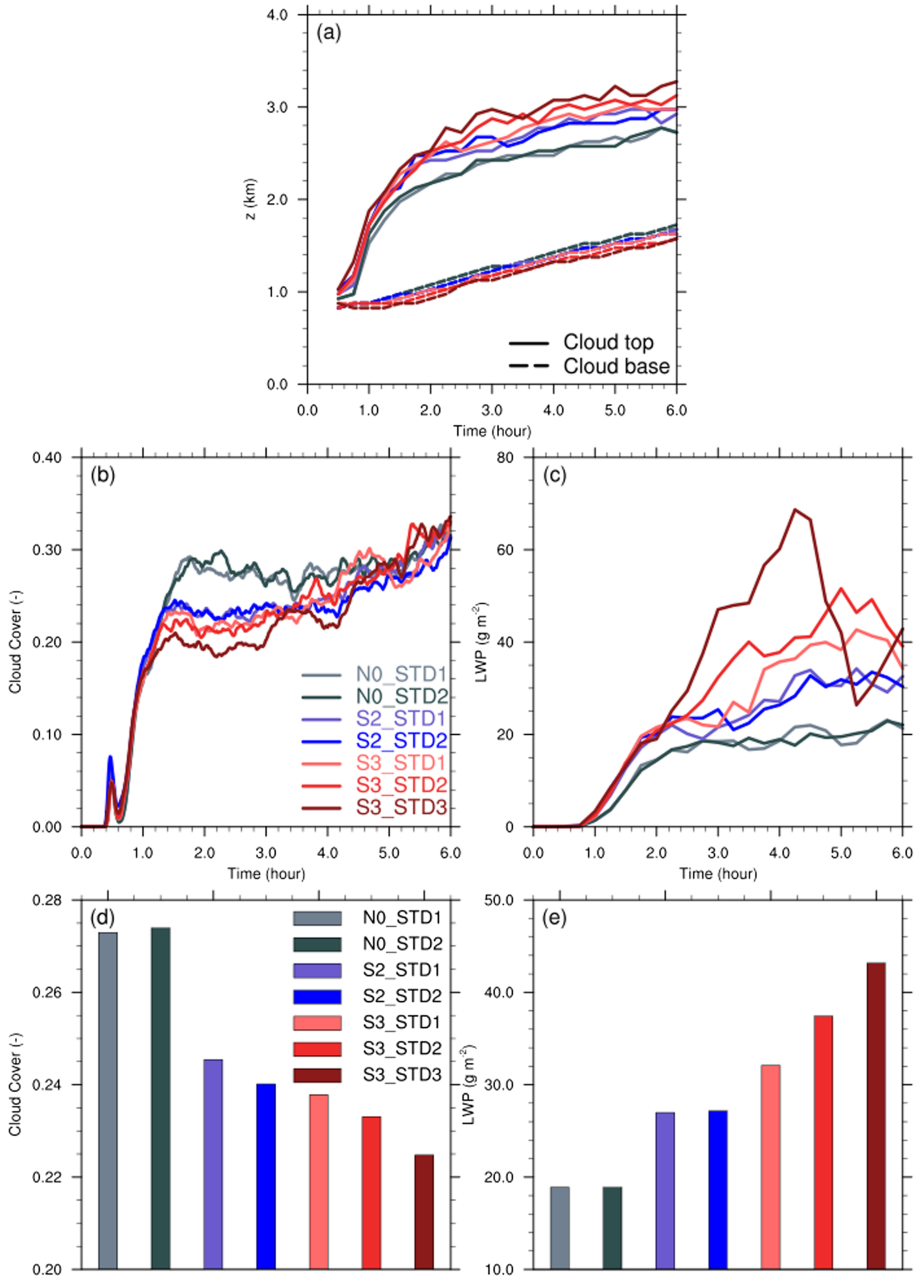

Figure 5. Temporal evolution of the domain-averaged (a) cloud-base height (solid curve) and cloud-top height (dashed curve), (b) cloud cover, (c) LWP; domain- and time-averaged (d) cloud cover, and (e) LWP, these quantities were averaged over the time period $t = 2$ to 6 hr.

surface compared to other cases indicating that the soil moisture heterogeneity has limited impact on the vertical profile of moisture flux.

Vertical profiles of the liquid water mixing ratio and liquid water flux shown in Figure 9c and Figure 9f, respectively, indicate a clear impact of soil moisture heterogeneity (both structure and variance) on the formation of clouds. The amount of liquid water increases from the unstructured to strongly structured cases, and the altitude where the liquid water peak occurs also increases with stronger structure (Figure 9c). Interestingly, for the weak and unstructured cases, liquid water profiles are identical between cases with different soil moisture variance. However, in the strongly structured cases (S3 cases), the amount of liquid water and the elevation where the liquid water peak occurs increase with increasing variance. Similar characteristics are also found in profiles of liquid water flux, which will be discussed in section 3.3.

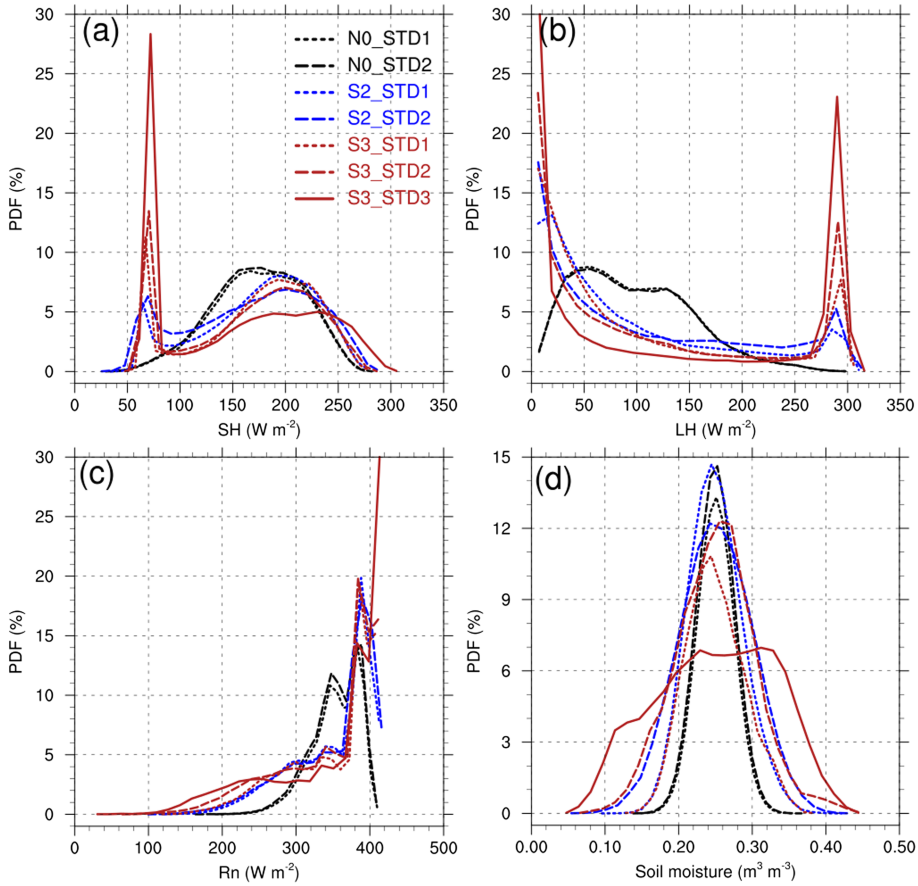

Figure 6. Probability density function of surface (a) sensible heat flux, (b) latent heat flux, (c) net radiation flux, and (d) soil moisture. Tweny-five bins were used for the probability distribution function. These quantities were averaged over the time period $t = 2$ to 6 hr.

3.2.2. Vertical Profiles of Variances

Figure 10 depicts the domain- and time-averaged vertical profiles of the variance of horizontal wind velocity, vertical wind velocity, potential temperature, specific humidity, and cloud liquid water. We apply the scale decomposition scheme commonly used to isolate mesoscale circulation impacts (Hussain & Reynolds, 1970; Kang & Ryu, 2016; Patton et al., 2005; Sullivan et al., 2000), to inspect if the given two-dimensional soil moisture heterogeneity induces any mesoscale circulation related processes that are strong enough to influence the boundary layer characteristics.

The structured soil moisture cases show a higher variation in the horizontal wind velocity throughout the boundary layer, which can be attributed to the increased mesoscale contribution (Figure 10a). Strongly structured cases (S3 cases) show the largest horizontal wind variations close to ground surface and near the CBL top, indicating the strengthening of the induced mesoscale circulation. However, the vertical wind velocity variance from the structured soil moisture case is weaker compared to the unstructured case (Figure 10b). This characteristic is due to the effect of the well-developed mesoscale circulation on the distribution of vertical velocity in the CBL. After the establishment of the mesoscale circulation, the strong and narrow updrafts are located principally over the dry patches, while the weak and broad downdrafts are dominating over the wet patches. The compensating downdrafts form due to the convergence near the CBL top and thus suppress thermals from rising over the wet patches. Similar results were also reported by Kang and Davis (2008).

Domain- and time-averaged vertical profiles of potential temperature variance and specific humidity variance are shown in Figure 10c and Figure 10d respectively. Significant differences among cases are not only shown in the cloud layer ($z > 1.5$ km) but also in the layers below the boundary layer top. The case with a larger soil moisture variance shows larger peak values of total potential temperature variance at both the ground

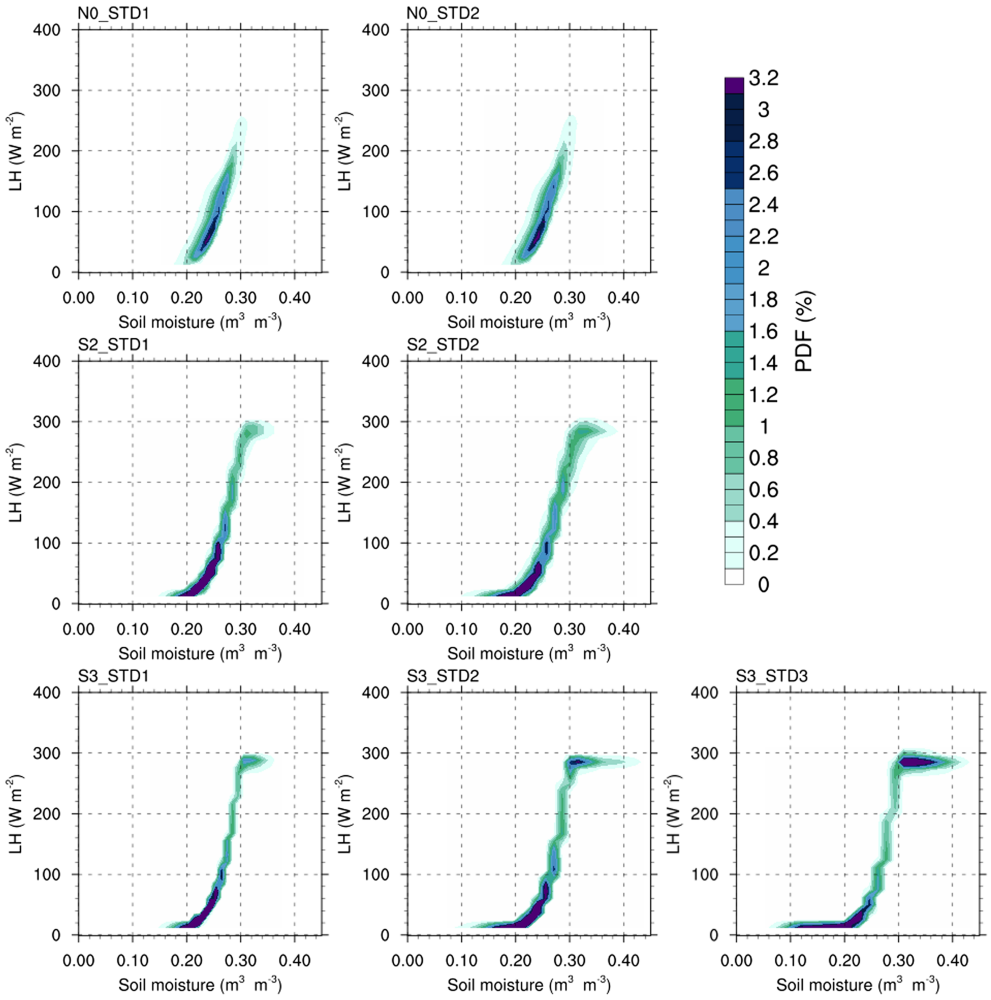

Figure 7. Bivariate probability density functions between latent heat flux and soil moisture. The quantities were averaged over the time period t = 2 to 6 hr.

surface and the cloud layer (Figure 10c). Interestingly, the mesoscale contribution is less important than the contribution of turbulence scale to the total potential temperature variance. In this case, mesoscale circulations are not strong enough to influence the spatial variability of potential temperature in the CBL. This result is in contrast to Kang and Davis (2008) who found that the temperature variance profiles are highly influenced by the mesoscale circulation using a stripe-like heterogeneity pattern. The main reason is that Kang and Davis (2008) used a dry CBL configuration with the prescribed sensible heat forcing at the model bottom and without moisture in the atmosphere, which magnifies the influence of heterogeneous heating from the surface and leads to strong mesoscale circulation. Note that the turbulent eddies mostly dominate the vertical transport of heat, while both turbulent eddies and mesoscale motions control the vertical transport of moisture (Lee et al., 2019; Patton et al., 2005). This is the reason that mesoscale contributions are higher to specific humidity variance than to potential temperature variance.

There are two peaks in the profiles of specific humidity variance, one is near the entrainment zone and the other is at the cloud layer (Figure 10d). The values of total specific humidity variance increase with stronger structure. The mesoscale contribution is comparable to the turbulence scale contribution to the total specific humidity variance. Interestingly, for the three strongly structured cases (S3 cases), specific humidity variance increases with increasing soil moisture variance. This is consistent with the increase in latent heat flux with increasing soil moisture variance in the strongly structured cases (S3 cases). In addition, in the two weakly structured cases (S2 cases), the mesoscale contribution and the turbulence scale contribution compensate each other, leading to almost identical total specific humidity variances.

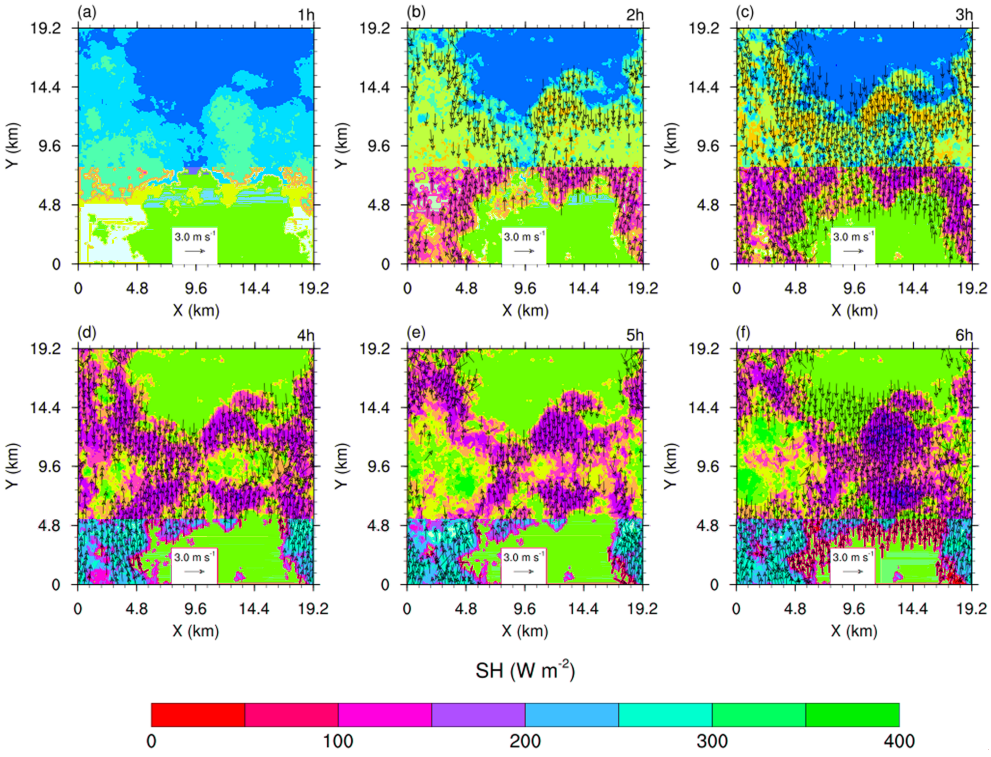

Figure 8. Spatial distribution of hourly averaged horizontal wind at the lowest model level (arrows) and surface sensible heat flux (shading) at hours (a) 1, (b) 2, (c) 3, (d) 4, (e) 5, and (f) 6 for case S3_STD3. Only wind vectors with velocity larger than 2 m/s are plotted.

Figure 10e depicts the domain- and time-averaged vertical profile of cloud liquid water variance. The peak value of liquid water variance increases with stronger structure, and the height of the peak value increases with stronger structure as well. In addition, for the strongly structured cases, the peak value of liquid water variance also increases with increasing soil moisture variance. The contribution of the mesoscale component

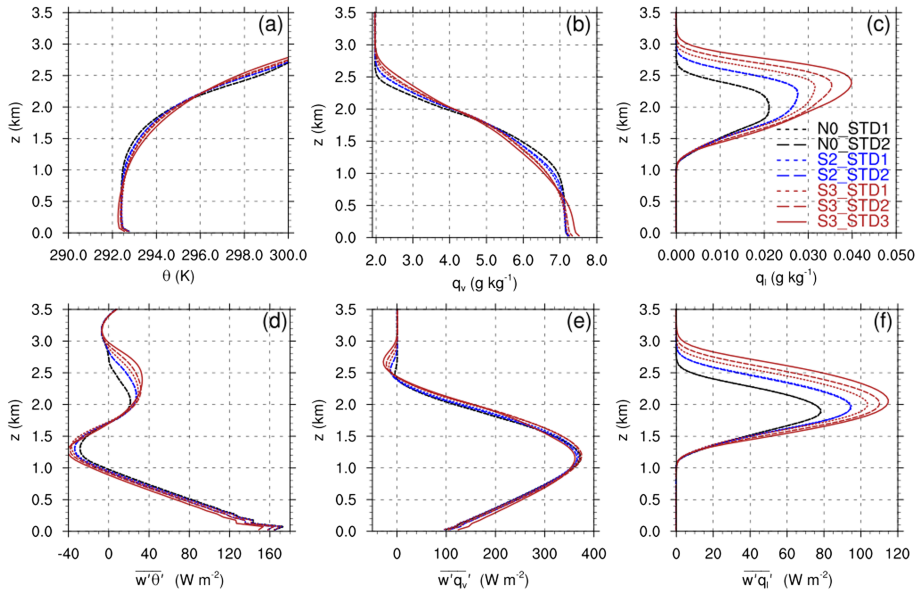

Figure 9. Vertical profiles of domain- and time-averaged (over t = 2 to 6 hr) (a) potential temperature, (b) specific humidity, (c) cloud liquid water mixing ratio, (d) buoyancy flux, (e) water vapor flux, and (f) liquid water flux.

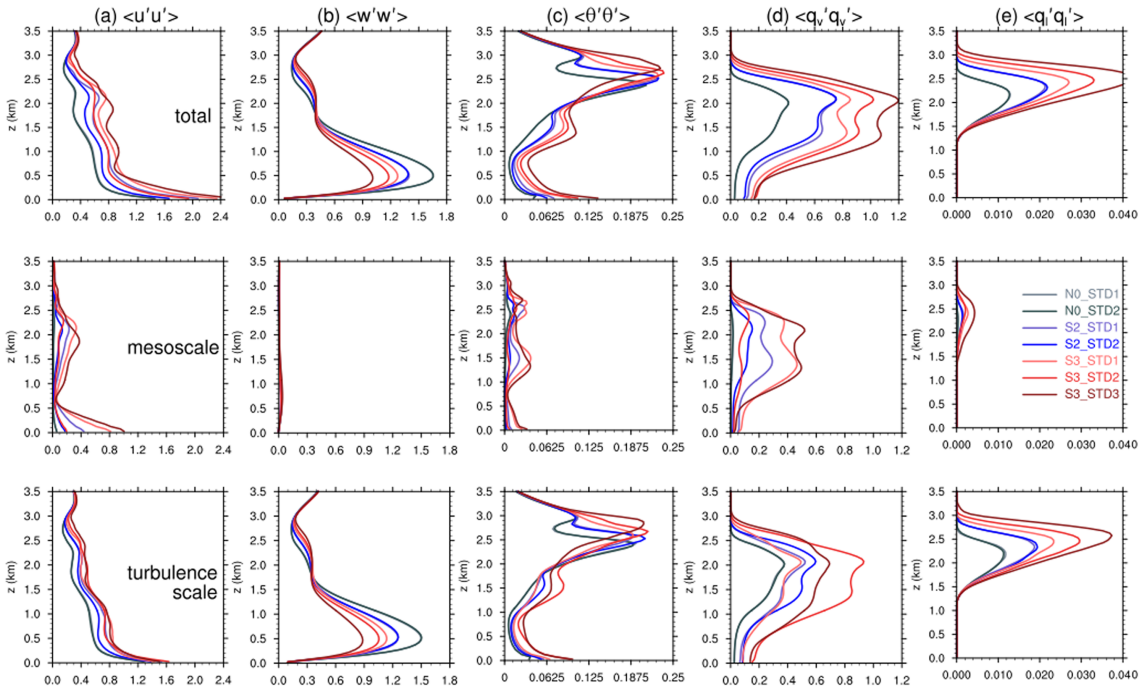

Figure 10. Vertical profiles of (left column) horizontal wind velocity variance, (second column) vertical wind velocity variance, (third column) potential temperature variance, (fourth column) specific humidity variance, and (fifth column) cloud liquid water variance. The total variance (top row) is then decomposed into mesoscale (middle row) and turbulence scale contributions (bottom row). The vertical profiles are averaged in space over the domain and time over $t = 2$ to 6 hr.

is minimal compared with the turbulence scale component to the total liquid variance. The soil moisture heterogeneity in terms of soil moisture structure and spatial variance not only impacts the profile of specific humidity variance but also impacts on the profile of cloud liquid water variance. The mechanisms will be discussed in the following section.

3.3. Cloud Properties

Figure 5a shows the domain-averaged cloud base and cloud top height. The cloud top/cloud base height are taken as the absolute value, that is, the highest/lowest height where somewhere in the entire atmospheric column a grid cell with liquid water is present. The increase in cloud base and cloud top height is attributable to the warming and drying of the CBL due to the CBL growth and the persistent heating from the surface. It is interesting to note that the cloud top height increases with stronger structure, while the cloud base height slightly decreases with stronger structure. Thus, the cloud depth increases with stronger structure. For the strongly structured cases (S3 cases), the cloud top height increases with increasing soil moisture variance, while cloud base height decreases with increasing soil moisture variance. However, cloud base and cloud top heights are almost identical in weak (S2 cases) and unstructured cases (N0 cases) even having different soil moisture variances. Cloud base height decreases with increasing soil moisture variance in strongly structured cases due to the decrease in boundary layer height with increasing soil moisture variance in strongly structured cases.

Figure 5b depicts the temporal evolution of the domain-averaged total cloud cover. The cloud fraction is calculated based on an all-or-nothing scheme, which does not account for fractional cloud cover at a subgrid scale. Clouds started to form after 30 min of simulation time. The cloud cover rises rapidly during the first hour after formation reaching its first peak and then increases slowly. The first peak values of the cloud cover of the heterogeneous cases are smaller than that of the homogeneous case; the peak value of cloud cover is about 20% in the structured cases, while the value is 30% in the unstructured cases. Overall the cloud cover in the unstructured cases is larger than that in the structured case. Additionally, the time when the cloud cover

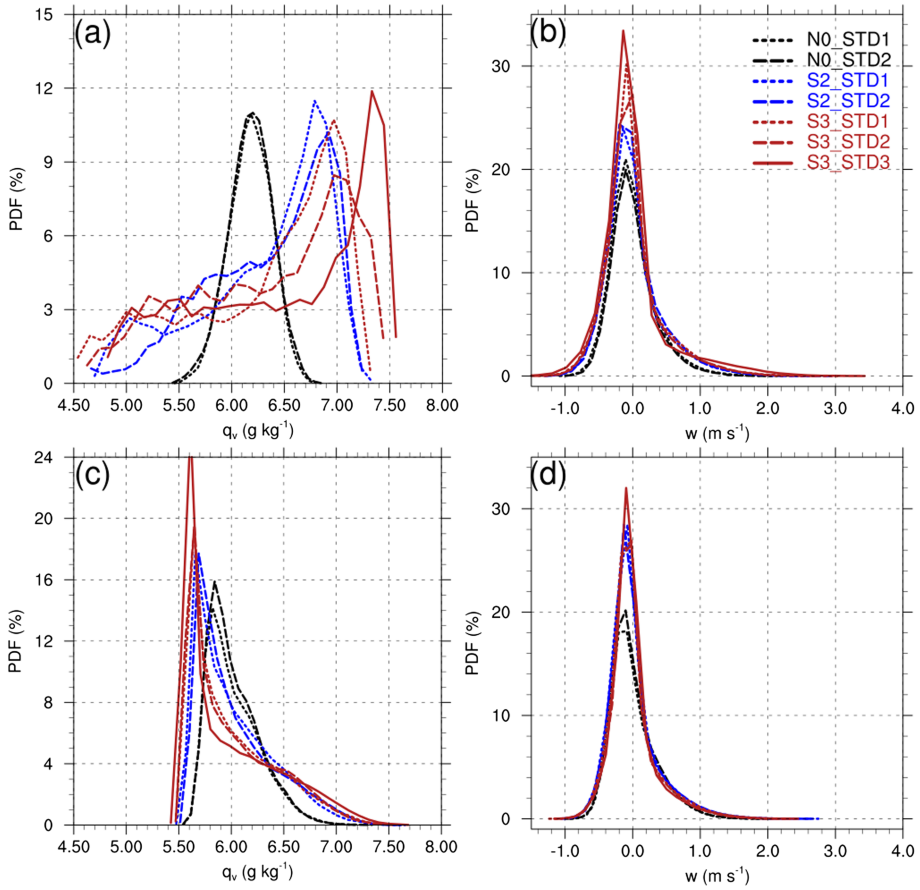

Figure 11. Probability distribution function of (a, c) water vapor specific humidity and (b, d) vertical wind velocity at the boundary layer top. Twenty-five bins were used for the probability density function. The quantities of (a) and (b) were averaged over the time period t = 2 to 6 hr after the mesoscale circulation were well developed (c) and (d) were averaged over the time period t = 1 to 2 hr before the mesoscale circulation were well established.

reaches its first peak in the structured case is earlier than that in the unstructured case, and the time difference is about 25 min (Figure 5b).

Domain- and time-averaged total cloud cover and LWP are shown in Figure 5d and Figure 5e, respectively. The total cloud cover decreases with stronger structure from ~0.27 in the unstructured cases to about 0.22 in case S3_STD3. However, the LWP increases with stronger structure from 18.9 g/m^2 in the unstructured cases to 43.3 g/m^2 in case S3_STD3. The relative increase is as much as 129%. This result is consistent with the change in cloud thickness (Figure 5a), which increases with stronger structure. Interestingly, LWPs are almost identical for varying variance for the weak and unstructured cases, while in the strongly structured cases, LWPs increase significantly with increasing soil moisture variance.

Figure 4 shows the spatial distributions of time-averaged LWPs. In unstructured cases, shallow cumulus clouds with low LWP are evenly distributed and cover a large fraction of the whole domain. However, in the structured cases, several deep cumulus clouds with high LWP are covering only a small fraction of the entire domain. This result explains why the LWP is higher in the structured case, while total cloud cover is lower than that in the unstructured case. This feature is consist with results reported by convective organization, which suggests that higher convective organization potential leads to the presence of deeper and larger clouds (Tobin et al., 2012; White et al., 2018). Moreover, clouds mainly form over the dry areas because of the induced mesoscale circulations. Soil moisture evaporates into the atmosphere over the wet surface and is advected to the dry surface by the induced mesoscale circulation (Kang, 2016; van Heerwaarden & de Arellano, 2008). The larger sensible heat flux over dry surface leads to more rising air parcels capable of forming clouds.

In the CBL, buoyant thermals rising from the land surface penetrate the boundary layer and overshoot into the free atmosphere (Stull, 1988). Moisture at the boundary layer top, which is a widely used indicator to quantify the potential for cloud formation (Ek & Holtslag, 2004; Gentine et al., 2013; van Heerwaarden & de Arellano, 2008), is taken up by the thermals as the surface is the only moisture source. Figure 11a shows the PDF of water vapor specific humidity at the boundary layer top after the mesoscale circulations are well developed (averaged over time period $t = 2$ to 6 hr). The peak values of specific humidity PDFs shift toward larger values with stronger structure. This means that air parcels at the boundary layer top are more moist in case of strongly structured case compared to the weak and unstructured case. That is, moist pools are formed in strongly structured case. Furthermore, there is a larger percentage of air parcels at the boundary layer top with vertical velocities >1.0 m/s in the structured case than that in the unstructured case resulting a pronounced tail in the distribution. As shown in Figure 11b, the vertical velocity at the boundary layer top is not larger than 2.1 m/s in unstructured cases, while the maximum vertical velocities are as large as 3.5 m/s in structured cases. This means that the air parcels are more energetic and more easily reach the lifting condensation level. Thus, it is not surprising that LWP increases with stronger structure. The reason why LWPs in strongly structured cases increase with increasing soil moisture variance is attributable to the specific humidity at the boundary layer top. As shown in Figure 11a, there is a larger percentage of moist air parcels in case of higher soil moisture variance. However, the LWPs in the weak and unstructured cases do not increase with increasing soil moisture variance, which may due to the heterogeneity that is not structured enough to influence the specific humidity at the boundary layer top. Before the mesoscale circulations are established, the peak values of specific humidity PDFs are around 5.6 g/kg (Figure 11c), which are much smaller than the peak values after the mesoscale circulations are well developed. In addition, the shifting of peak values toward larger values is not obvious between different cases. Before the mesoscale circulations are established (Figure 11d), the vertical velocities are also smaller than vertical velocities after the mesoscale circulations are well developed. This means energetic moist pools have not been formed before mesoscale circulations are well established.

4. Summary and Conclusions

We presented general characteristics of the development of a CBL and shallow cumulus clouds and their response to the spatial variation of soil moisture in a mesoscale domain of 19.2×19.2 km^2. A series of numerical experiments were performed applying LES simulations with prescribed initial atmospheric profiles and two-dimensional heterogeneous soil moisture distributions. The domain means of soil moisture were preserved, while the spectral slope of the power law model of soil moisture increased from 0 to −3, that is, from unstructured and weak structure to strong structure, and also spatial variances were different.

The heterogeneous soil moisture distribution resulted in heterogeneities in surface heat and moisture fluxes influencing surface energy partitioned into sensible heat flux and latent heat flux. The higher soil moisture variance, the more available energy were partitioned into latent heat flux in the structured cases. The heterogeneity in the surface sensible heat flux triggered mesoscale circulations in the CBL, resulting in flow divergence over the wet patches and converges over the dry patch close to the land surface. The mesoscale circulation, in turn, influenced surface heat fluxes due to the variation in horizontal wind velocity and variations in the vertical gradients of temperature and humidity. That is the interactions between surface heterogeneity and induced mesoscale circulations is also the reason why domain averages of surface sensible and latent heat fluxes differ, while the domain averages of soil moisture are identical.

The soil moisture heterogeneity impacted the vertical profiles of the boundary layer states, fluxes, and variances via surface energy partitioning and induced mesoscale circulations. The most significant modifications occurred in the profiles of liquid water and liquid water flux. The profiles of potential temperature, specific humidity, buoyancy flux, and specific humidity flux were also influenced but not significantly. We decomposed the total variance into a mesoscale and turbulence scale component to verify if the induced mesoscale circulations are strong enough to influence the CBL and the cumulus cloud characteristics. Our results indicate that the mesoscale circulations had a strong influence on the vertical profiles of horizontal velocity variance and specific humidity variance.

Interestingly, the total cloud cover decreased with stronger structure, while the LWP increased with stronger structure. In strongly structured cases (S3 cases), the total cloud cover decreased with increasing soil

moisture variance, while the LWP increased with increasing soil moisture variance. More available energy is partitioned into latent heat in case of high soil moisture variance, thus more moisture evaporates into the atmosphere. Moreover, there were more air parcels with high vertical velocity at the boundary layer top in the structured case than in the unstructured case. Thus, there are more opportunities for moist updrafts in the structured case to penetrate the boundary layer and reach the lifting condensation level. This suggests that it is easier to develop deep convection over the structured surface than over the unstructured surface. Interestingly, soil moisture variance only plays a role in strongly structured case not in weak or unstructured case, which indicates soil moisture variance and spectral slope work together in the surface energy partitioning and the cloud formation.

One might argue that there are other factors that contribute to impact on the intensity ofinduced mesoscale circulation, the CBL structure, and the development of shallow convection, for example, the background wind, wind direction relative to the heterogeneity, wind shear, and atmospheric conditions. Note that some processes were excluded in this study, such as the cloud shading-induced surface heterogeneities and the changes in soil moisture due to evaporation. In addition, the soil moisture heterogeneity scale, which is of the order of the half domain size in S3 cases, and the double-periodic boundary conditions might deflect statistics. Thus, a much more systematic investigation on the impact of the land surface heterogeneity will be carried out in the future.

Acknowledgments
BMBF sponsored this work through the research program "High Definition of Clouds and Precipitation for Advancing Climate Prediction" (HD (CP)^2, grant no. 01LK1506D). We gratefully acknowledge the computing time allowed by the German Climate Computing Centre (Deutsche Klimarechenzentrum, DKRZ) on the HPC system Mistral and the Jülich Supercomputing Centre (JSC) on the HPC system JURECA. Simulation output is available through the institutional repository (https://datapub.fz-juelich.de/slts/shcu/).

References

Avissar, R., & Schmidt, T. (1998). An evaluation of the scale at which ground-surface heat flux patchiness affects the convective boundary layer using large-eddy simulations. *Journal of the Atmospheric Sciences*, *55*(16), 2666–2689. https://doi.org/10.1175/1520-0469(1998)055<2666:AEOTSA>2.0.CO;2

Bosman, P. J. M., van Heerwaarden, C. C., & Teuling, A. J. (2018). Sensible heating as a potential mechanism for enhanced cloud formation over temperate forest. *Quarterly Journal of the Royal Meteorological Society*. https://doi.org/10.1002/qj.3441

Chen, F., & Avissar, R. (1994). Impact of land-surface moisture variability on local shallow convective cumulus and precipitation in large-scale models. *Journal of Applied Meteorology*, *33*(12), 1382–1401. https://doi.org/10.1175/1520-0450(1994)033<1382:IOLSMV>2.0.CO;2

Chlond, A., Böhringer, O., Auerswald, T., & Müller, F. (2014). The effect of soil moisture and atmospheric conditions on the development of shallow cumulus convection: A coupled large-eddy simulation-land surface model study. *Meteorologische Zeitschrift*, *23*(5), 491–510. https://doi.org/10.1127/metz/2014/0576

Cioni, G., & Hohenegger, C. (2017). Effect of soil moisture on diurnal convection and precipitation in large-eddy simulations. *Journal of Hydrometeorology*, *18*(7), 1885–1903. https://doi.org/10.1175/JHM-D-16-0241.1

Colella, P., & Woodward, P. R. (1984). The piecewise parabolic method (PPM) for gas-dynamical simulations. *Journal of Computational Physics*, *54*(1), 174–201. https://doi.org/10.1016/0021-9991(84)90143-8

Desai, A. R., Davis, K. J., Senff, C. J., Ismail, S., Browell, E. V., Stauffer, D. R., & Reen, B. P. (2006). A case study on the effects of heterogeneous soil moisture on mesoscale boundary-layer structure in the Southern Great Plains, U.S.A. Part I: Simple Prognostic Model. *Boundary-Layer Meteorology*, *119*(2), 195–238. https://doi.org/10.1007/s10546-005-9024-6

Dickinson, R. E. (1984). Modeling evapotranspiration for three-dimensional global climate models. In *Climate Processes and Climate Sensitivity* (pp. 58–72). Washington, DC: American Geophysical Union.

Dipankar, A., Stevens, B., Heinze, R. R., Moseley, C., Zängl, G., Giorgetta, M., & Brdar, S. (2015). Large eddy simulation using the general circulation model ICON. *Journal of Advances in Modeling Earth Systems*, *7*, 963–986. https://doi.org/10.1002/2015MS000431

Dörnbrack, A., & Schumann, U. (1993). Numerical simulation of turbulent convective flow over wavy terrain. *Boundary-Layer Meteorology*, *65*(4), 323–355. https://doi.org/10.1007/BF00707032

Ek, M. B., & Holtslag, A. A. M. (2004). Influence of soil moisture on boundary layer cloud development. *Journal of Hydrometeorology*, *5*(section 2), 86–99. https://doi.org/10.1175/1525-7541(2004)005<0086:IOSMOB>2.0.CO;2

Findell, K. L., & Eltahir, E. A. B. (2003a). Atmospheric controls on soil moisture—Boundary layer interactions. Part I: Framework development. *Journal of Hydrometeorology*, *4*(3), 552–569. https://doi.org/10.1175/1525-7541(2003)004<0552:ACOSML>2.0.CO;2

Findell, K. L., & Eltahir, E. A. B. (2003b). Atmospheric controls on soil moisture—Boundary layer interactions. Part II: Feedbacks within the continental United States. *Journal of Hydrometeorology*, *4*(3), 570–583. https://doi.org/10.1175/1525-7541(2003)004<0570:ACOSML>2.0.CO;2

Gentine, P., Ferguson, C. R., & Holtslag, A. A. M. (2013). Diagnosing evaporative fraction over land from boundary-layer clouds. *Journal of Geophysical Research: Atmospheres*, *118*, 8185–8196. https://doi.org/10.1002/jgrd.50416

Golaz, J.-C., Jiang, H., & Cotton, W. R. (2001). A large-eddy simulation study of cumulus clouds over land and sensitivity to soil moisture. *Atmospheric Research*, *59-60*, 373–392. https://doi.org/10.1016/S0169-8095(01)00113-2

Hadfield, M. G., Cotton, W. R., & Pielke, R. A. (1991). Large-eddy simulations of thermally forced circulations in the convective boundary layer. Part I: A small-scale circulation with zero wind. *Boundary-Layer Meteorology*, *57*(1), 79–114. https://doi.org/10.1007/BF00119714

Hadfield, M. G., Cotton, W. R., & Pielke, R. A. (1992). Large-eddy simulations of thermally forced circulations in the convective boundary layer. Part II: The effect of changes in wavelength and wind speed. *Boundary-Layer Meteorology*, *58*(4), 307–327. https://doi.org/10.1007/BF00120235

Han, C., Brdar, S., Raasch, S., & Kollet, S. (2019). Large-eddy simulation of catchment-scale circulation. *Quarterly Journal of the Royal Meteorological Society*, *145*(720), 1218–1233. https://doi.org/10.1002/qj.3491

Heße, F., Prykhodko, V., Schlüter, S., & Attinger, S. (2014). Generating random fields with a truncated power-law variogram: A comparison of several numerical methods. *Environmental Modelling & Software*, *55*, 32–48. https://doi.org/10.1016/j.envsoft.2014.01.013

Huang, H. Y., & Margulis, S. A. (2013). Impact of soil moisture heterogeneity length scale and gradients on daytime coupled land-cloudy boundary layer interactions. *Hydrological Processes*, *27*(14), 1988–2003. https://doi.org/10.1002/hyp.9351

Huang, H.-Y., & Margulis, S. A. (2011). Investigating the impact of soil moisture and atmospheric stability on cloud development and distribution using a coupled large-eddy simulation and land surface model. *Journal of Hydrometeorology*, *12*(5), 787–804. https://doi.org/10.1175/2011JHM1315.1

Hussain, A. K. M. F., & Reynolds, W. C. (1970). The mechanics of an organized wave in turbulent shear flow. *Journal of Fluid Mechanics*, *41*(2), 241–258. https://doi.org/10.1017/S0022112070000605

Kang, S.-L. (2016). Regional Bowen ratio controls on afternoon moist convection: A large eddy simulation study. *Journal of Geophysical Research: Atmospheres*, *121*, 14,056–014,083. https://doi.org/10.1002/2016JD025567

Kang, S.-L., & Bryan, G. H. (2011). A large-eddy simulation study of moist convection initiation over heterogeneous surface fluxes. *Monthly Weather Review*, *139*(9), 2901–2917. https://doi.org/10.1175/MWR-D-10-05037.1

Kang, S.-L., & Davis, K. J. (2008). The effects of mesoscale surface heterogeneity on the fair-weather convective atmospheric boundary layer. *Journal of the Atmospheric Sciences*, *65*(10), 3197–3213. https://doi.org/10.1175/2008JAS2390.1

Kang, S.-L., & Ryu, J.-H. (2016). Response of moist convection to multi-scale surface flux heterogeneity. *Quarterly Journal of the Royal Meteorological Society*, *142*(698), 2180–2193. https://doi.org/10.1002/qj.2811

Lee, J. M., Zhang, Y., & Klein, S. A. (2019). The effect of land surface heterogeneity and background wind on shallow cumulus clouds and the transition to deeper convection. *Journal of the Atmospheric Sciences*, *76*(2), 401–419. https://doi.org/10.1175/JAS-D-18-0196.1

Lilly, D. K. (1962). On the numerical simulation of buoyant convection. *Tellus*, *14*(2), 148–172. https://doi.org/10.1111/j.2153-3490.1962.tb00128.x

Margulis, S. A., & Entekhabi, D. (2001). Feedback between the land surface energy balance and atmospheric boundary layer diagnosed through a model and its adjoint. *Journal of Hydrometeorology*, *2*(6), 599–620. https://doi.org/10.1175/1525-7541(2001)002<0599:FBTLSE>2.0.CO;2

Maronga, B., & Raasch, S. (2013). Large-eddy simulations of surface heterogeneity effects on the convective boundary layer during the LITFASS-2003 experiment. *Boundary-Layer Meteorology*, *146*(1), 17–44. https://doi.org/10.1007/s10546-012-9748-z

Miura, H. (2007). An upwind-biased conservative advection scheme for spherical hexagonal–pentagonal grids. *Monthly Weather Review*, *135*(12), 4038–4044. https://doi.org/10.1175/2007MWR2101.1

Niyogi, D. S., Raman, S., & Alapaty, K. (1999). Uncertainty in the specification of surface characteristics. Part II: Hierarchy of interaction-explicit statistical analysis. *Boundary-Layer Meteorology*, *91*(3), 341–366. https://doi.org/10.1023/A:1002023724201

Patton, E. G., Sullivan, P. P., & Moeng, C.-H. (2005). The influence of idealized heterogeneity on wet and dry planetary boundary layers coupled to the land surface. *Journal of the Atmospheric Sciences*, *62*(7), 2078–2097. https://doi.org/10.1175/JAS3465.1

Pielke, R. A. (2001). Influence of the spatial distribution of vegetation and soils on the prediction of cumulus convective rainfall. *Reviews of Geophysics*, *39*(2), 151–177. https://doi.org/10.1029/1999RG000072

Raasch, S., & Harbusch, G. (2001). An analysis of secondary circulations and their effects caused by small-scale surface inhomogeneities using large-eddy simulation. *Boundary-Layer Meteorology*, *101*(1), 31–59. https://doi.org/10.1023/A:1019297504109

Richards, L. A. (1931). Capillary conduction of liquids through porous mediums. *Physics*, *1*(5), 318–333. https://doi.org/10.1063/1.1745010

Rieck, M., Hohenegger, C., & van Heerwaarden, C. C. (2014). The influence of land surface heterogeneities on cloud size development. *Monthly Weather Review*, *142*(10), 3830–3846. https://doi.org/10.1175/MWR-D-13-00354.1

Rochetin, N., Couvreux, F., & Guichard, F. (2017). Morphology of breeze circulations induced by surface flux heterogeneities and their impact on convection initiation. *Quarterly Journal of the Royal Meteorological Society*, *143*(702), 463–478. https://doi.org/10.1002/qj.2935

Santanello, J. A., Dirmeyer, P. A., Ferguson, C. R., Findell, K. L., Tawfik, A. B., Berg, A., et al. (2018). Land–atmosphere interactions: The LoCo perspective. *Bulletin of the American Meteorological Society*, *99*(6), 1253–1272. https://doi.org/10.1175/BAMS-D-17-0001.1

Santanello, J. A., Friedl, M. A., & Ek, M. B. (2007). Convective planetary boundary layer interactions with the land surface at diurnal time scales: Diagnostics and feedbacks. *Journal of Hydrometeorology*, *8*(5), 1082–1097. https://doi.org/10.1175/JHM614.1

Schrodin, R., & Heise, E. (2002). A new multi-layer soil model. Retrieved from Offenbach, Germany:

Seifert, A., & Beheng, K. D. (2001). A double-moment parameterization for simulating autoconversion, accretion and selfcollection. *Atmospheric Research*, *59-60*, 265–281. https://doi.org/10.1016/S0169-8095(01)00126-0

Shen, S., & Leclerc, M. Y. (1995). How large must surface inhomogeneities be before they influence the convective boundary layer structure? A case study. *Quarterly Journal of the Royal Meteorological Society*, *121*(526), 1209–1228. https://doi.org/10.1002/qj.49712152603

Siebesma, A. P., Bretherton, C. S., Brown, A., Chlond, A., Cuxart, J., Duynkerke, P. G., et al. (2003). A Large eddy simulation intercomparison study of shallow cumulus convection. *Journal of the Atmospheric Sciences*, *60*(10), 1201–1219. https://doi.org/10.1175/1520-0469(2003)60<1201:ALESIS>2.0.CO;2

Sommeria, G., & Deardorff, J. W. (1977). Subgrid-scale condensation in models of nonprecipitating clouds. *Journal of the Atmospheric Sciences*, *34*(2), 344–355. https://doi.org/10.1175/1520-0469(1977)034<0344:SSCIMO>2.0.CO;2

Stull, R. B. (1988). *An introduction to boundary layer meteorology*. Dordrecht: Kluwer Academic Publishers.

Sühring, M., Maronga, B., Herbort, F., & Raasch, S. (2014). On the effect of surface heat-flux heterogeneities on the mixed-layer-top entrainment. *Boundary-Layer Meteorology*, *151*(3), 531–556. https://doi.org/10.1007/s10546-014-9913-7

Sullivan, P. P., McWilliams, J. C., & Moeng, C.-H. (2000). Simulation of turbulent flow over idealized water waves. *Journal of Fluid Mechanics*, *404*, 47–85. https://doi.org/10.1017/S0022112099006965

Taylor, C. M., Gounou, A., Guichard, F., Harris, P. P., Ellis, R. J., Couvreux, F., & De Kauwe, M. (2011). Frequency of Sahelian storm initiation enhanced over mesoscale soil-moisture patterns. *Nature Geoscience*, *4*(7), 430–433. https://doi.org/10.1038/ngeo1173

Tobin, I., Bony, S., & Roca, R. (2012). Observational evidence for relationships between the degree of aggregation of deep convection, water vapor, surface fluxes, and radiation. *Journal of Climate*, *25*(20), 6885–6904. https://doi.org/10.1175/JCLI-D-11-00258.1

van Heerwaarden, C. C., & de Arellano, J. V.-G. (2008). Relative humidity as an indicator for cloud formation over heterogeneous land surfaces. *Journal of the Atmospheric Sciences*, *65*(10), 3263–3277. https://doi.org/10.1175/2008JAS2591.1

van Heerwaarden, C. C., Mellado, J. P., & De Lozar, A. (2014). Scaling laws for the heterogeneously heated free convective boundary layer. *Journal of the Atmospheric Sciences*, *71*(11), 3975–4000. https://doi.org/10.1175/JAS-D-13-0383.1

Wan, H., Giorgetta, M. A., Zängl, G., Restelli, M., Majewski, D., Bonaventura, L., et al. (2013). The ICON-1.2 hydrostatic atmospheric dynamical core on triangular grids—Part 1: Formulation and performance of the baseline version. *Geoscientific Model Development*, *6*(3), 735–763. https://doi.org/10.5194/gmd-6-735-2013

White, B. A., Buchanan, A. M., Birch, C. E., Stier, P., & Pearson, K. J. (2018). Quantifying the effects of horizontal grid length and parameterized convection on the degree of convective organization using a metric of the potential for convective interaction. *Journal of the Atmospheric Sciences*, *75*(2), 425–450. https://doi.org/10.1175/JAS-D-16-0307.1

Zängl, G., Reinert, D., Rípodas, P., & Baldauf, M. (2015). The ICON (ICOsahedral Non-hydrostatic) modelling framework of DWD and MPI-M: Description of the non-hydrostatic dynamical core. *Quarterly Journal of the Royal Meteorological Society*, *141*(687), 563–579. https://doi.org/10.1002/qj.2378

Zhang, D., & Anthes, R. A. (1982). A high-resolution model of the planetary boundary layer—Sensitivity tests and comparisons with SESAME-79 data. *Journal of Applied Meteorology*, *21*(11), 1594–1609. https://doi.org/10.1175/1520-0450(1982)021<1594:AHRMOT>2.0.CO;2

Erratum

Due to typesetting errors, several figures in the originally published version of this manuscript were mislabeled. These errors have been corrected, and this may be considered the official version of record.